Geochemistry Geophysics Geosystems G3
AN ELECTRONIC JOURNAL OF THE EARTH SCIENCES
Published by AGU and the Geochemical Society

Article
Volume 9, Number 2
12 February 2008
Q02008, doi:10.1029/2007GC001814
ISSN: 1525-2027

Characteristics of ambient seismic noise as a source for surface wave tomography

Yingjie Yang and Michael H. Ritzwoller

Center for Imaging the Earth's Interior, Department of Physics, University of Colorado, Boulder, Colorado 80309-0390, USA (yingjie.yang@colorado.edu)

[1] Interstation cross correlations of ambient seismic noise from 1 year of continuous data at periods between 6 and 50 s are used to study the origin of the ambient noise using stations located in Europe, southern Africa, Asia, and three regions within North America. The signal-to-noise ratios (SNR) of Rayleigh waves for positive and negative correlation time lags at periods of 8, 14, 25 and 50 s are used to determine the azimuthal distribution of strong ambient noise sources. Ambient noise in both the primary (10–20 s) and secondary microseism bands (5–10 s) comes dominantly from the directions of relatively nearby coastlines with stronger noise occurring in the Northern Hemisphere in northern winter and in the Southern Hemisphere in southern winter, consistent with the hypothesis that oceanic microseisms are generating this noise. The observed differences in the directivity of noise in the primary and secondary microseism bands are the consequence of propagation and attenuation, rather than the location of generation. At intermediate and long periods (>20 s), there is much less seasonal variation in both signal strength and directivity. We argue that our results are explained most simply by near-coastal sources rather than deep ocean sources at all periods. Although the dominant ambient noise sources are distributed inhomogeneously in azimuth, strong ambient noise emerges from most directions when using recordings that are 1 year in duration. Simulations illustrate that this is what ensures the accuracy of the empirical Green's functions and ambient noise tomography.

Components: 8563 words, 14 figures.

Keywords: ambient seismic noise; cross correlations; Green's functions; tomography.

Index Terms: 7255 Seismology: Surface waves and free oscillations; 7270 Seismology: Tomography (6982, 8180).

Received 4 September 2007; **Revised** 17 November 2007; **Accepted** 30 November 2007; **Published** 12 February 2008.

Yang, Y., and M. H. Ritzwoller (2008), Characteristics of ambient seismic noise as a source for surface wave tomography, *Geochem. Geophys. Geosyst.*, *9*, Q02008, doi:10.1029/2007GC001814.

1. Introduction

[2] Theoretical and experimental research has shown that the cross correlation of ambient noise records from two receivers provides an estimate of the empirical Green's function between the receivers [*Weaver and Lobkis*, 2001, 2004; *Derode et al.*, 2003a; *Snieder*, 2004; *Larose et al.*, 2005]. In seismology, two types of signals have been considered to form random wavefields. The first is seismic coda, which results from the multiple scattering of seismic waves by small-scale inhomogeneities [e.g., *Aki and Chouet*, 1975; *Paul et al.*, 2005]. The second is ambient seismic noise. Ambient noise, in contrast with seismic coda, has the advantage that it does not depend on earth-

quake occurrence and can be recorded at any time and any location.

[3] Recently, surface wave tomography for Rayleigh waves based on the empirical Green's functions obtained from cross correlations of ambient seismic noise has been applied successfully to real data at regional scales, such as in the western United States [*Shapiro et al.*, 2005; *Sabra et al.*, 2005; *Moschetti et al.*, 2007; *Lin et al.*, 2008], South Korea [*Cho et al.*, 2007], Tibet [*Yao et al.*, 2006], New Zealand [*Lin et al.*, 2007], Iceland [*Gudmundsson et al.*, 2007], and southern Africa (Y. Yang et al., Crustal and uppermost mantle structure in southern Africa revealed from ambient noise and teleseismic tomography, submitted to *Geophysical Journal International*, 2007, hereinafter referred to as Yang et al., submitted manuscript, 2007), and at continental scales, such as in Europe [*Yang et al.*, 2007] and North America [*Bensen et al.*, 2007b]. The basic assumption underlying ambient noise tomography is that ambient seismic noise can be considered to be composed of randomly distributed wavefields when taken over sufficiently long times, such as a year. A perfectly random distribution of the sources of ambient noise would result in symmetric cross correlations with energy arriving at both positive and negative correlation lag times, usually referred to as the causal and acausal arrivals. In practice, however, significant asymmetry of the cross correlations is often observed, which results from stronger or closer ambient noise sources directed radially away from one station than the other. Although *Derode et al.* [2003b] showed experimentally that inhomogeneous source distributions have lesser effects on the travel times of the waves than on their signal-to-noise ratios, such source distributions may interfere at some level with the ability to obtain reliable Green's functions and measure dispersion curves on them. A better understanding of the origin of ambient noise sources and their temporal and spatial distribution is needed, therefore, to ensure that ambient noise tomography is being developed on a firm footing.

[4] Ambient seismic noise in the short-period band (<20 s), commonly referred to as microseisms, is considered to be related to the interaction of ocean swells with the seafloor near coastlines. Two strong peaks of the short-period seismic noise are typically observed in the primary (10–20 s) and secondary (5–10 s) microseism bands. The exact generation mechanism of the microseisms is not completely understood, but it is commonly believed that the primary microseism involves direct interaction of ocean swells with the shallow seafloor [*Hasselmann*, 1963], and the secondary microseism, with double-frequency signals relative to the primary microseism, is generated by the nonlinear interaction between the two same frequency primary waves but propagating in opposite directions [*Longuet-Higgins*, 1950]. Such nonlinear interaction of two oppositely propagating waves may arise near the center of cyclonic depression at the deep sea or near the costal regions where the direct waves and coastline-reflected waves interfere. Long-period seismic noise, referred to as earth "hum," is observed in the continuous background free oscillations in low-frequency seismic spectra [*Nawa et al.*, 1998]. This term is usually reserved for motions with periods above 100 s. Early studies attributed the long-period noise to atmospheric motions [*Tanimoto and Um*, 1999; *Ekstrom*, 2001], but more recent studies [*Tanimoto*, 2005; *Rhie and Romanowicz*, 2004, 2006] suggest that the origin of the long-period noise is more likely related to so-called ocean infragravity waves, a long-period ocean gravity wave. *Rhie and Romanowicz* [2004] proposed that the generation of long-period seismic noise involves a three stage atmosphere-ocean-seafloor coupling process.

[5] The procedure to use long-duration cross correlations to study the long-range correlation properties of ambient seismic noise was developed by *Stehly et al.* [2006]. They applied the method to about 20 stations in each of California, the eastern United States, Europe, and Tanzania and found that ambient noise in the secondary microseism band is seasonally stable and emerges predominantly from nearby coastlines. In contrast, the primary microseism and longer-period ambient noise (below 40 s period) vary seasonally in similar ways and emerge from directions that may not be toward the local coasts. This observation appeared to them to sever the hypothesized physical link between the primary and secondary microseisms, and called into question the commonly believed casual relation between these waves. These authors argue that the cause of the primary microseism and the longer-period ambient noise is ocean wave activity in deep water. This conclusion is at variance with the study of *Rhie and Romanowicz* [2006], which is based on detailed observations performed on seismic arrays in Japan and California during a large storm in the Pacific. Rhie and Romanowicz conclude that at all periods, from the secondary microseism at several seconds period to earth hum at 240 s, ocean wave energy is coupled to the solid earth predominantly

near coastlines. They argue that nonlinear ocean wave-wave interactions near the coast generate long-period energy, which propagates globally both as seismic waves in the solid earth and infragravity waves in the ocean which can then liberate their energy to the solid earth later, elsewhere. This mechanism may imply that ambient noise is not uniformly distributed in time or space, which may vitiate assumptions that underlie ambient noise tomography, however.

[6] In this study, we follow the methodology of *Stehly et al.* [2006], but apply the method to a much larger station set in Europe, southern Africa, Tibet, and North America using 12 months of ambient noise data over a broad period band from 6 to 50 s, which covers the microseism band as well as longer-period noise. By analyzing the strength and quality of the cross correlations in different seasons, directions, and period bands, we address three principal questions. First, we consider whether the primary and secondary microseisms behave differently on average and, hence, may be physically decoupled. Second, we ask whether the observations are consistent with generation in shallow coastal waters at all periods or require a deepwater source at long periods. Finally, we consider whether the resulting azimuthal distribution of ambient seismic noise is sufficiently homogeneous when taken over long times for ambient noise tomography to be successful. We focus on Rayleigh waves, so the results for Love waves may differ. We proceed by first looking at results from Europe, and then bring in results using arrays in southern Africa, Tibet, and North America.

[7] Throughout the paper, we will refer to the "source" of ambient noise, and our use of this term requires clarification. By "source location," we refer to the place or places where seismic waves within the solid earth are generated. The proximate cause of the seismic waves may be the interaction of gravity waves in the ocean with the seafloor. Identification of the ultimate cause of ambient noise involves a regress of physical mechanisms that may have involved the generation of ocean gravity waves, the generation of large ocean storms from the interaction of winds with the ocean surface, storm formation in the atmosphere, differential solar forcing, and so on. Seismic waves, however, are blind to all processes that occurred prior to their generation, although the location of their formation, their frequency content, seasonal variability, and radiation pattern may provide clues about earlier processes. Thus, by the "source," "source location," "generation" and "cause," we will refer only to that place where and mechanism by which the seismic waves are generated.

[8] Finally, it is important to acknowledge at the outset that the method of source characterization that we use is ambiguous and the arguments presented herein are qualitative in nature. The method is only capable of determining the relative direction to the principal source locations observed at an array, and inferences drawn about absolute locations must be made on the basis of plausibility and simplicity. We attempt to make that clear when simplicity based on the principle is assumed.

2. Initial Analysis: Cross Correlations of Ambient Noise in Europe

[9] We use continuous vertical component seismic data from ~125 stations from the Global Seismic Network (GSN) and the Virtual European Broadband Seismic Network (VEBSN) (Figure 1) over the 12 months of 2004. The data processing procedure applied here is similar to that described at length by *Bensen et al.* [2007a]. Raw seismic data are processed one day at a time for each station after being decimated to 1 sample per second, and are band-pass filtered in the period band from 5 to 50 s after the daily trend, the mean and the instrument response are removed. Filtered daily data are then normalized in time and whitened in this frequency band to remove earthquake signals and instrumental irregularities prior to performing cross correlation. Daily cross correlations are computed between all station pairs and are then added to one another or stacked to produce two 5-month and one 1-year time series. The two 5-month stacks are centered on January and July respectively; namely, months 11, 12, 1, 2, 3 and months 5, 6, 7, 8, 9. The 5-month stacks are used to investigate the seasonal variability of the ambient noise source.

[10] Examples of 12-month cross correlations are plotted in Figure 2 with the corresponding path segments shown in the bottom map. For each cross correlation, surface wave signals coming from the two opposite directions between the stations appear at positive (casual component) and negative (acausal component) correlation time lag, respectively. The incoming directions of seismic noise contributing to the positive components are marked with arrows showing the directions of propagation along each path segment in Figure 2f. The positive components are for waves coming mostly from the

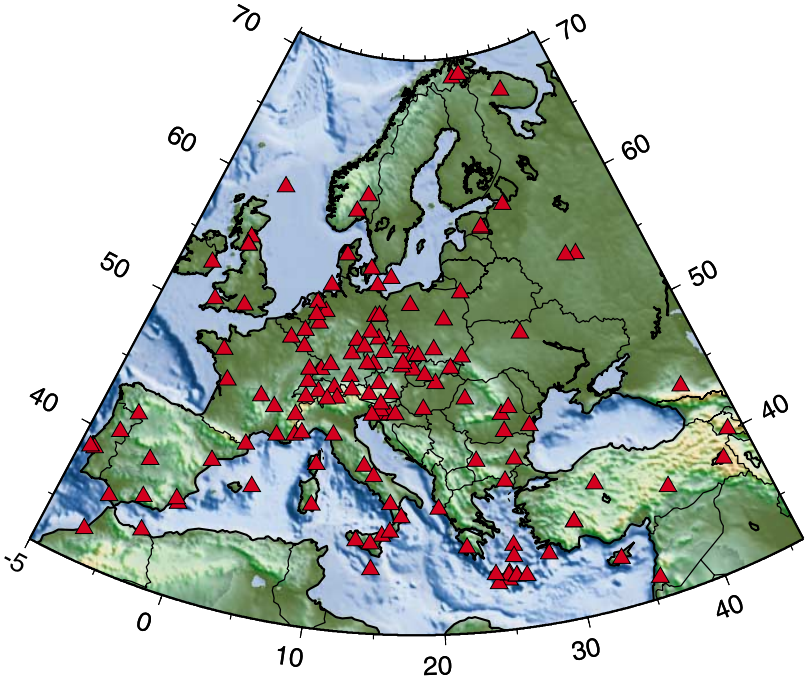

Figure 1. Broadband seismic stations in Europe used in this study, marked by red triangles.

northerly direction. The amplitude of the causal and acausal components depends on the strength and density of sources of ambient noise in line with the stations. Although signals coming from opposite directions sample the same structure between a station pair, the source characteristics, such as distance, strength, duration, frequency content and so on, may be very different on the two opposite sides. Thus the resulting cross correlations are often asymmetric, as illustrated in Figure 2, and these properties may be period-dependent. For example, the higher-amplitude arrivals in Figure 2 are generally from the north, i.e., at positive lag. The negative lag components for station pairs ECH-TUE and DSB-TUE are nearly flat, indicating that there is relatively little energy arriving from the southeast. There is, however, substantial energy at negative lags for the pairs GRFO-TUE, MORC-TUE and KWP-TUE, resulting from waves coming from the southwest. There is also apparently a difference in frequency content at positive and negative lags. The best example is probably MORC-TUE, where a clear low-frequency precursor appears at positive lag (coming from the northeast), which is missing at negative lag.

[11] To demonstrate the frequency content of the signals in Figure 2, we plot in Figure 3 normalized amplitude spectra of the positive (Figures 3f–3j) and negative (Figures 3a–3e) lag components of the corresponding cross-correlation time series. In each case, 1000-s time series are used to compute the spectrum, starting from zero lag. The lower curve in each panel is the normalized spectrum of trailing noise contained in the 1000 s time window starting at ±1000 s lag time, which is always well removed from the surface wave signals. To illustrate the frequency-dependent characteristics of ambient noise sources, we divide the entire frequency band into three subbands: namely, low-frequency noise LFN (0–0.05 Hz), the primary microseism band MS1 (0.05–0.1 Hz), and the secondary microseism band MS2 (0.1–0.2 Hz). For cross correlations between the station pairs GRFO-TUE, MORC-TUE and KWP-TUE, there are strong low-frequency noise signals on the positive components (Figures 2b–2d and 3g–3i), which come from the northeast quadrant (Figure 2f). For the cross correlations ECH-TUE and DSB-TUE, strong microseismic noise signals are observed on the positive components (Figures 2a, 2e, 3f, and 3j), coming from the northwest quadrant, but little energy is observed in the low-frequency band. The lack of high-frequency noise from a particular direction probably is a consequence of a distant source region. The frequency-dependent characteristics of noise signals in strength and incoming direction are discussed in more detail in

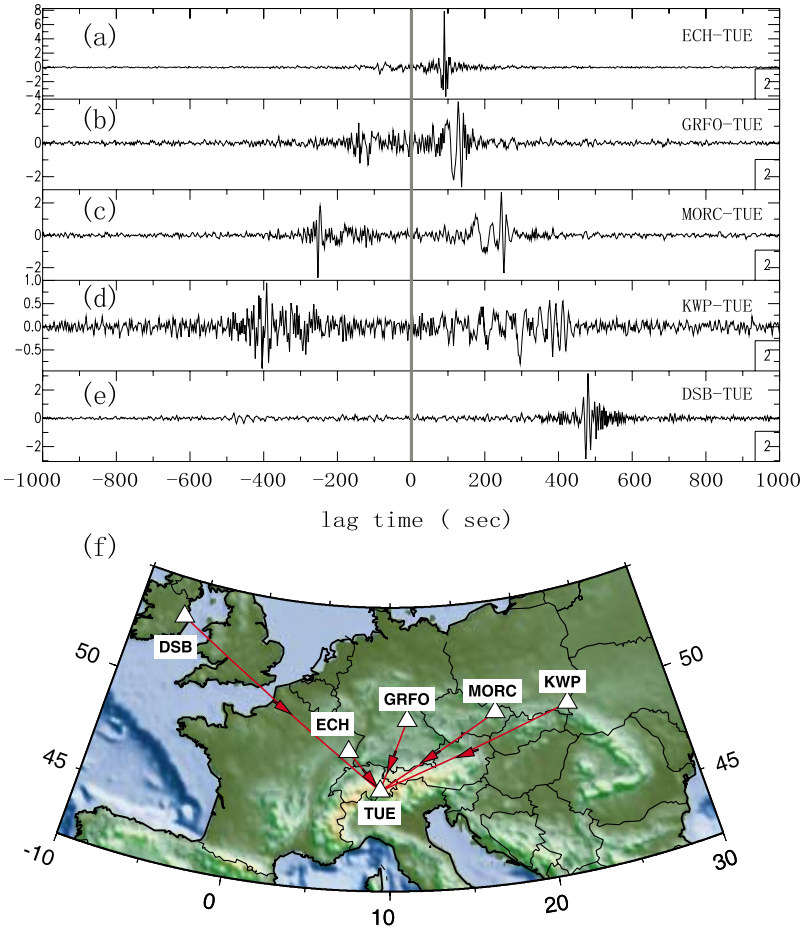

Figure 2. (a–e) Examples of 12-month broadband cross correlations. The bold gray line indicates the zero arrival time. Cross correlations are ordered by interstation distances with station names indicated in each waveform panel. Note that the cross correlations are often asymmetric. (f) Locations of the stations (white triangles) and path segments for the corresponding cross correlations, with arrows marking the incoming directions of noise contributing to the positive components.

the next section for Europe and then in subsequent sections for elsewhere in the world.

[12] To evaluate the quality and amplitude of the cross correlations quantitatively, we calculate the period-dependent signal-to-noise (SNR) for the positive and negative components of each cross correlation. SNR is defined as the ratio of the peak amplitude within a time window containing the surface wave signals to the root-mean-square of the noise trailing the signal arrival window. The signal window is determined using the arrival times of Rayleigh waves at the minimum and maximum periods of the chosen period band (6 to 50 s) using the global 3-D shear velocity model of *Shapiro and Ritzwoller* [2002]. The period dependence of SNR is determined by applying a series of narrow band-pass (ranging form 5 to 10 mHZ) filters centered on a grid of periods from 6 to 50 s. Figure 4a shows an example of a positive component broad-band cross correlation (eighth panel) along with seven narrow band-pass filtered time series. Rayleigh wave signals show up clearly in each of these bands. Figure 4b displays the corresponding SNR as a function of period. SNR in this example (and generally) peaks in the primary microseism band (10–20 s), around 14 s period.

[13] We use SNR as a proxy to estimate the strength of noise sources, which is similar to the normalized amplitude used by *Stehly et al.* [2006] to estimate noise strength because the root-mean-square of the noise trailing the signal arrival is similar for the cross correlations within the same seismic array. For each cross correlation, we have two SNR measurements for positive and negative components, respectively, to indicate the noise energy flux from the two opposite directions along

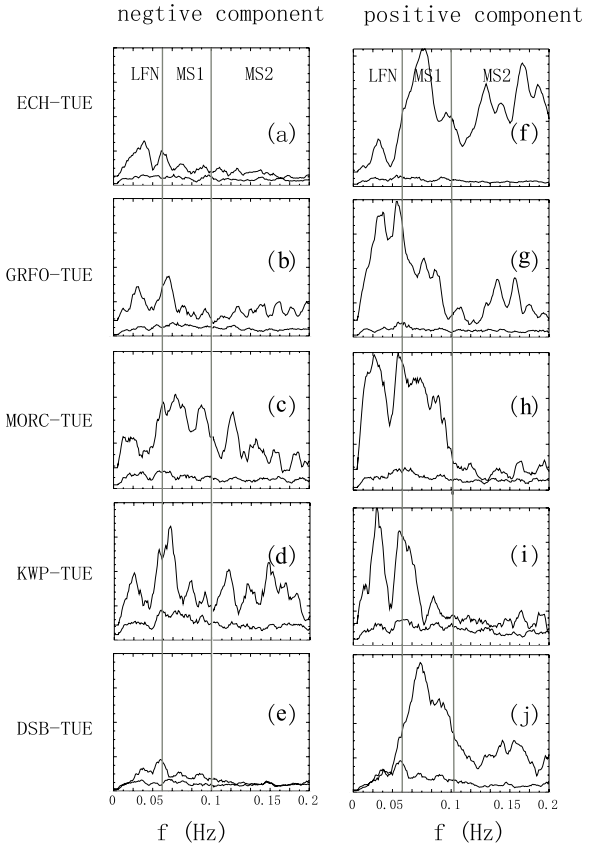

Figure 3. Normalized spectra of (a–e) negative and (f–j) positive components of the cross correlations shown in Figure 2. The three frequency bands of LFN, MS1 and MS2 delineated by the bold lines correspond to the infragravity band and the primary and secondary microseism bands.

the great circle linking the stations. Combining all the cross correlations within a seismic array, we can estimate noise energy flux from all azimuthal directions. Since we do normalization in both the time and spectral domain on continuous noise time series before performing cross correlations, the estimate of noise strength from SNR can only tell us the relative strength as a function of azimuth.

3. Sources of Ambient Noise Observed in Europe

[14] To investigate the directions of the incoming ambient noise systematically, we plot in Figure 5 the azimuthal distribution of SNR for the positive and negative components of each cross correlation at 8, 14, 25 and 50 s period in the northern winter and northern summer of 2004. Each line points in the direction from which the energy arrives (i.e., it points to the source location) and its length is proportional to the SNR. At 8 and 14 s period, lines drawn to the edge of circle represent a SNR of at least 80, and at 25 s and 50 s the lines to the circle's edge mean the SNR is at least 60.

[15] The periods of 8 and 14 s are near the center of the secondary (5–10 s) and primary (10–20 s) microseism bands, respectively. The strength and directionality of ambient noise at these two periods are shown in Figure 5 to be very similar to one another, and they demonstrate similar, strong seasonal dependence with much stronger noise arriving in the northern winter than in the northern summer. The seasonal variation in the strength of ambient noise, with the noise level being much higher in winter than in summer, is consistent with higher sea states in winter than in summer in the north Atlantic [*Webb*, 1998]. In the winter, at both periods the strongest energy is arriving from the northwest quadrant. The strongest arrivals are also from the northwest quadrant during the summer, but the arrivals from the north are less energetic. The one exceptional difference between the patterns of energy arrival at 8 and 14 s is stronger noise from the northeast quadrant at 14 s period during the northern summer.

[16] The patterns of energy arriving at the longer periods of 25 and 50 s are quite distinct from waves in the microseism band. These waves display little seasonal variability and the azimuthal patterns of energy arriving at these periods are very similar to one another, with the strongest energy arriving from the northeast at both periods and seasons. The only appreciable difference between 25 and 50 s is that the SNR at 25 s is higher than at 50 s period.

[17] Figures 6 and 7 illustrate possible source locations by back-projecting along a great circle arc for each station pair with a SNR > 20. In the secondary microseism band (~8 s period) shown in Figure 6, source directions are broadly distributed to the west and northwest of Europe. In our view, the simplest distribution of source locations would be for them to occur near the European coast, ranging from west of Spain to the European Arctic coast of the Baltic peninsula in winter. The alternative would be for the sources to emanate from a much larger area, to lie in deep water spanning the entire North and Central Atlantic. We view this as implausible. In northern summer, the range of azimuths for the high SNR sources diminishes to near coastal France, England, the North Sea region, and coastal Norway. At 14 s period during the summer, seismic energy also arrives to the Euro-

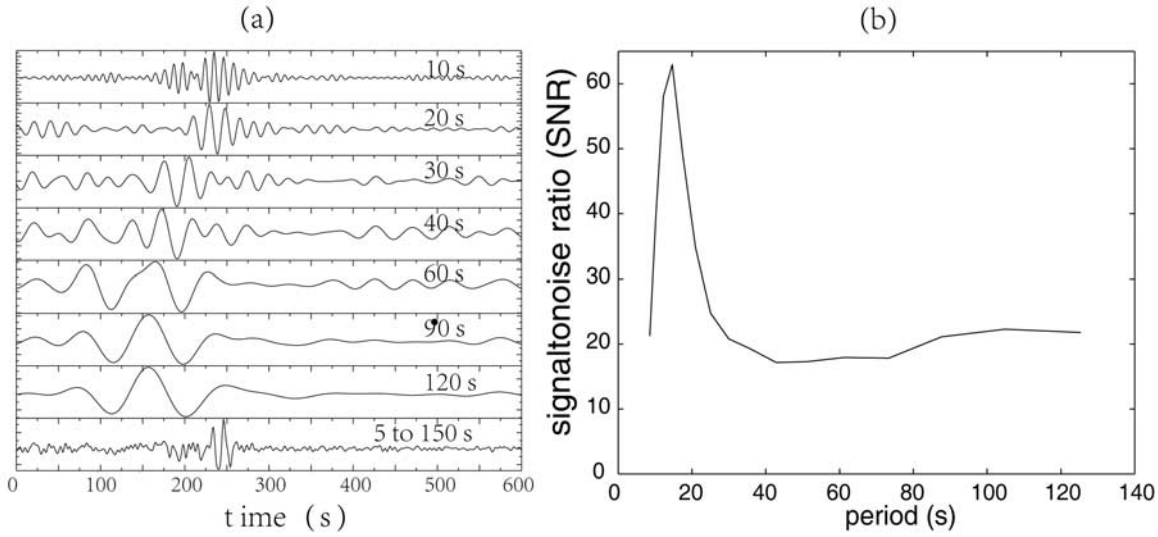

Figure 4. (a) Example of a broadband positive component cross correlation using 12 months of data between stations IBBN (Ibbenbueren, Germany) and MOA (Molln, Austria). The broadband signal (5–150 s) is shown in the eighth panel. Other panels are narrow band-pass filtered waveforms with the central periods indicated in each panel. (b) Calculated SNR values from each narrow band-passed filtered waveforms versus period.

pean stations from the northeast, apparently having emanated from east of Asia. Again, the simplest explanation would be for the sources to occur along the east Asian coastline, predominantly off of China, Korea/Japan, and Russia. The sole significant difference between 8 and 14 s period is these arrivals from the east Asian coast at 14 s during the northern summer. This can be understood as a wave propagation phenomenon, with the 8 s waves having been attenuated more than those at 14 s. Similarly, east Asian earthquake waves observed in Europe are enriched at 14 s relative to 8 s wave energy. The 8 s Rayleigh waves similarly cannot propagate coherently over transcontinental distances.

[18] At 25 s and 50 s, illustrated in Figure 7, the patterns of the back-projected rays are nearly identical with each other in summer and winter. The strongest arriving energy is from the northeast, probably having originated along the western Pacific rim. Again, we view the shallow water source location to be more plausible than the deep water sources distributed over a much larger area. There are fewer large amplitude arrivals from the western quadrants. Those that exist probably have originated near the European coast for the same reason. Although deep water sources for the longer-period arrivals cannot be ruled out on the basis of the seismic evidence alone, the spatial distribution of sources would have to be very diffuse and we are unaware of any evidence for this.

[19] Our analysis of ambient noise directionality in Europe indicates little significant difference between the directional content of energy arriving in the two microseism bands. The differences that do exist can be attributed to the fact that the longer-period primary microseismic energy (~14 s) propagates farther than secondary microseismic energy (~8 s), and therefore can arise from the Pacific rim of Asia. In addition, the principle of simplicity argues for concentrated near-coastal source locations as opposed to diffuse mid-oceanic source locations over a much larger area. However, the method we use cannot locate noise sources unambiguously, and the results in Europe may differ from those elsewhere in the world. Thus, in the following sections, we analyze ambient noise directionality in southern Africa, Tibet, and North America.

4. Further Analysis: Cross Correlations of Ambient Noise in Southern Africa and Asia

[20] The stations used in this analysis are shown in Figure 8. Twelve months of data are processed using stations from two PASSCAL experiments; the Southern Africa Seismic Experiment (SASE) with data from 1998 and the Eastern Syntaxis Tibet Experiment with data from 2003 and 2004. We process data exactly as for the European stations, but obtain results only at periods of 8, 14 and 25 s because the arrays are smaller and longer-period

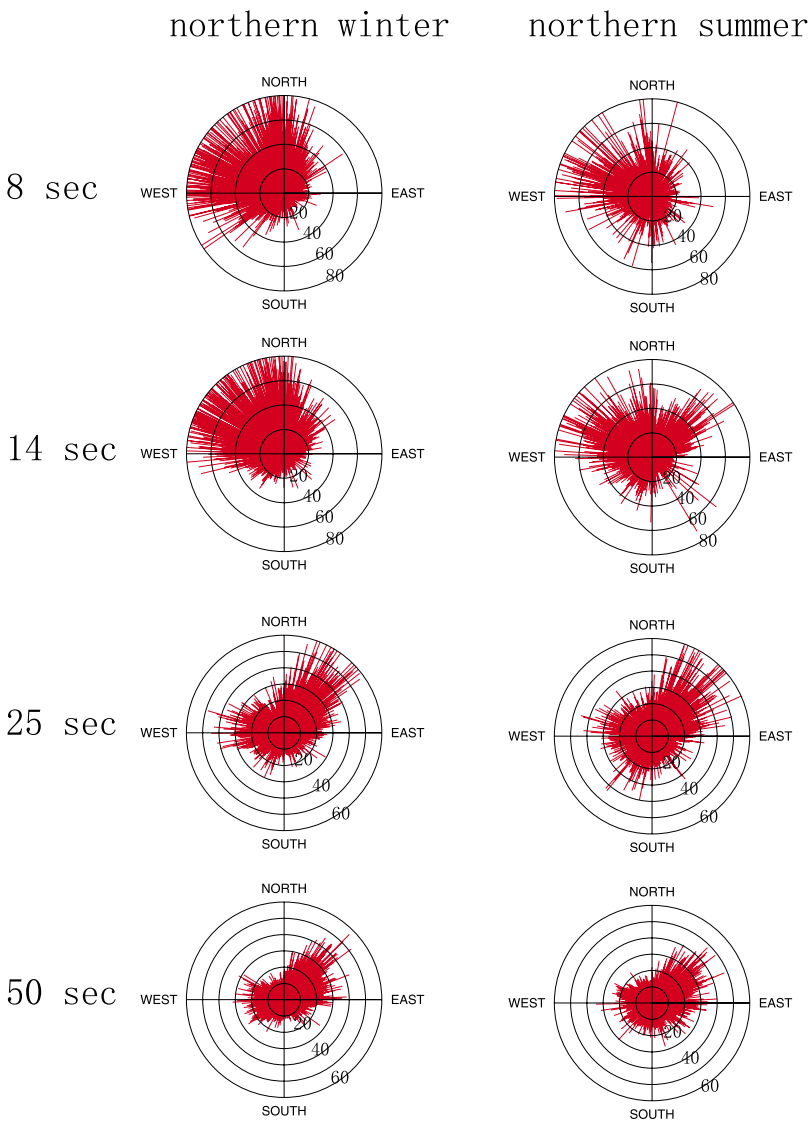

Figure 5. Azimuthal distribution of SNR of 5-month stacks during the (left) northern winter and (right) summer at periods 8, 14, 25 and 50 s taken from European seismic stations. SNR levels are indicted by the concentric circles with values shown in each of the diagrams.

results are less robust than in Europe. The azimuthal distribution of SNR from the southern African, Tibetan, and European stations are plotted in Figure 9 in both the northern summer and winter.

[21] Like in Europe, at 8 and 14 s period, considerable seasonal variability is observed both in southern Africa and Tibet. In Tibet, ambient noise is stronger in the northern winter than the northern summer and the principal directions of noise swing to the south in the northern summer. In understandable contrast to the observations in Europe, however, ambient noise is stronger at these periods in southern Africa during the northern summer (southern winter) than in the northern winter (southern summer) (Figures 9a–9d). Thus, at 8 and 14 s period, ambient noise is stronger in the local winter in most directions in all three locations. In southern Africa, the azimuthal content of noise emanating from the southern quadrants at these two periods is very similar to one another and there is less seasonal dependence. The simplest explanation is that ambient noise from the southern quadrants arrives from nearby coastlines having been generated there. Noise from the northern quadrants in southern Africa is different at 8 and 14 s, however, and there is a stronger seasonal dependence. Strong noise (SNR > 40) at 14 s arriving from the north and northwest to southern Africa during the northern winter, back-projects to the northern European coasts, similar to observa-

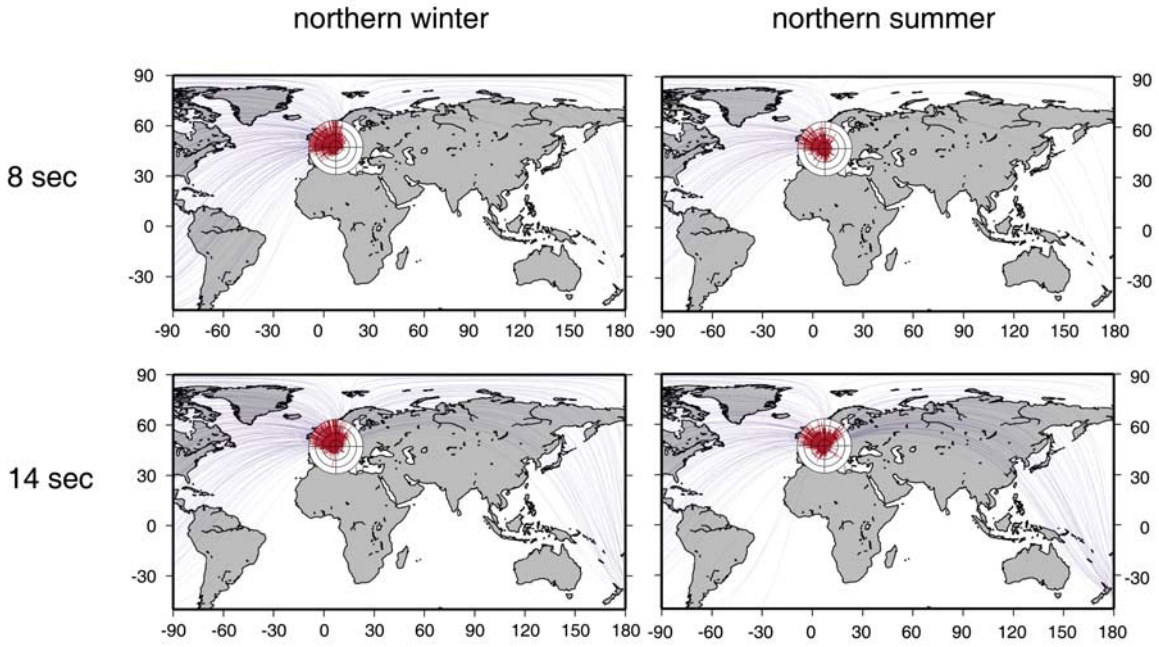

Figure 6. Back-projected great circle paths of cross correlations at periods of 8 and 14 s in the northern summer and winter with corresponding azimuthal distribution overplotted at the center of Europe. The great circle paths indicate the approximate locations along which noise sources constructively contribute to surface wave signals. Paths shown here have SNR > 20.

tions in Europe. Strong noise (SNR > 60) arriving at 14 s from the northeast, which is particularly strong in the northern summer, is more difficult to interpret. For example, as shown in Figure 9d, this noise back-projects to the east Asian coast similar to results from the European stations, but the Tibetan results indicate that the strongest noise there is coming from the southwest rather than

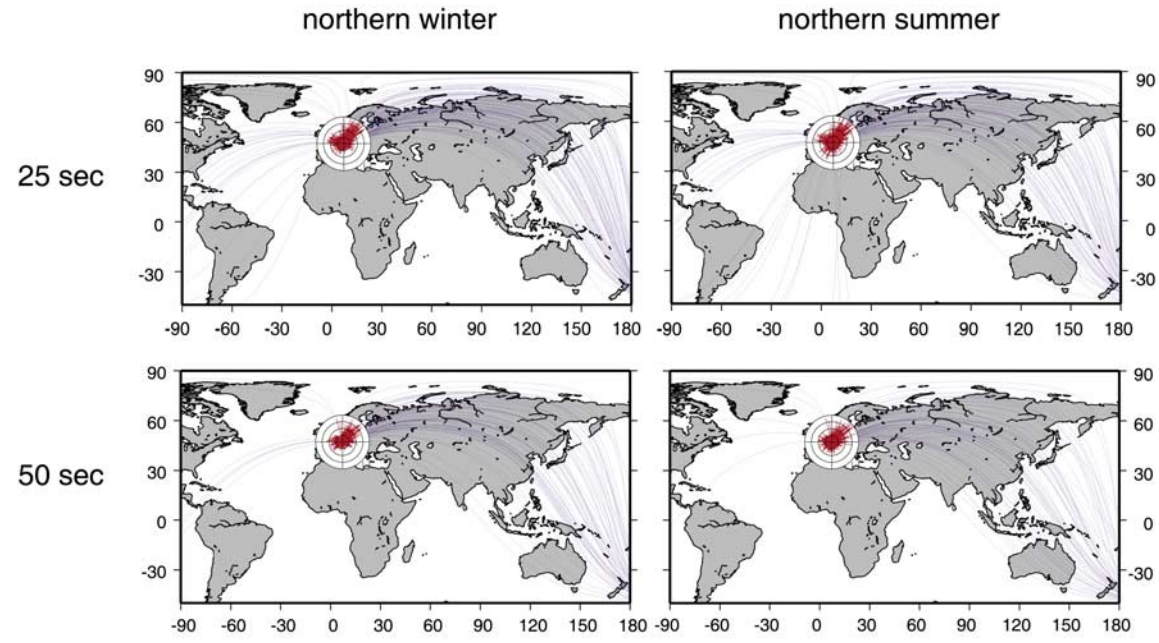

Figure 7. Same as Figure 6 but for periods of 25 and 50 s.

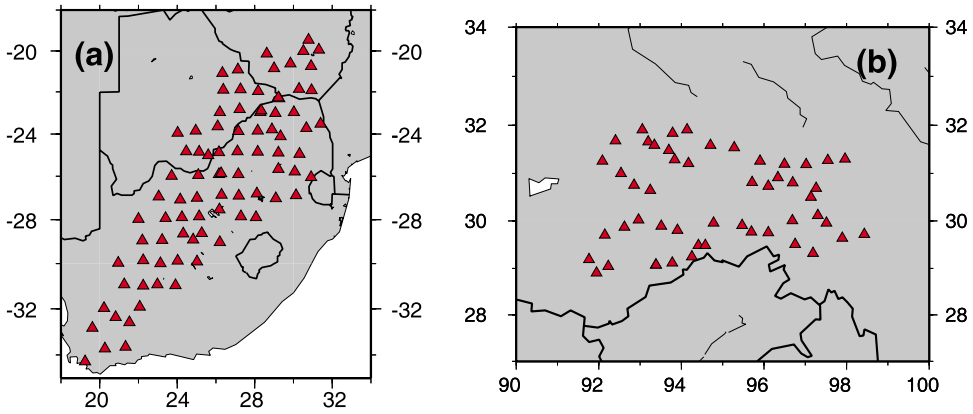

Figure 8. Stations used in southern Africa from the Southern African Seismic Experiment and Tibet from the Eastern Syntaxis Tibet Experiment.

the northeast. It is unlikely, therefore, that the strong arrivals at 14 s observed at the European and southern African stations emanate from a single source region in east Asia. We believe that it is more likely that the 14 s southern African energy finds its source near the African coast or perhaps along the coastlines of the Arabian Sea.

[22] These observations illustrate that the azimuthal patterns of microseismic energy arriving at these three locations display some common systematics, particularly as related to seasonal variability. Differences between the 8 s and 14 s observations again can be understood largely as propagation effects. The source locations of the noise arriving in these regions are largely distinct, however. It is, therefore, unlikely that large storms in the deep oceans are the direct source of microseismic energy at 14 s period, which is more likely to have been produced in relatively shallow near coastal waters. The seasonal variability of the microseisms, however, illustrates that large deep ocean storms are probably the cause of the ocean gravity wave energy that transforms to ambient seismic noise in shallow waters.

[23] At 25 s period, as in Europe, there is little seasonal dependence of the directionality of ambient noise in southern Africa and the azimuthal content of ambient noise at this period differs substantially with that at either 8 s or 14 s period. The southern African noise at this period is generally of larger amplitude than in Europe, probably because of higher sea states in the Southern Hemisphere, and is also more omnidirectional than in Europe, consistent with the source of the ambient noise occurring near the coast along much of southern Africa rather than in deep water to the south of Africa where sea states are highest. In Tibet, like Europe and southern Africa, the azimuthal distribution of incoming noise at 25 s differs substantially from 8 or 14 s period. However, unlike Europe or southern Africa, there is substantial seasonal variability, with strong noise coming from the southern quadrants in both the northern summer and winter but also from the north in the northern winter. The directions of arrival of strong noise in Europe, southern Africa, and Tibet at 25 s are not consistent with a single or small number of exceptionally strong source locations, but rather indicate that strong noise emerges at these arrays from many directions, presumably with a broad distribution of source locations. These observations are, therefore, at variance with a deep water source for ambient noise at 25 s period.

5. Further Analysis: Cross Correlations of Ambient Noise in North America

[24] We also use continuous seismic data from numerous stations in California, the eastern United States, Alaska and northwest Canada, processing them using the same methods as for the European, southern African, and Tibetan data. The stations are shown in Figure 10 and the results are presented at 8, 14, and 25 s in Figure 11.

[25] At 8 and 14 s period, results for the stations in the eastern United States and Alaska/Canada are straightforward. SNR is larger in the northern winter than the northern summer, but the directional dependence of noise is largely seasonally independent. In addition, the directional patterns at these periods are largely similar. In Alaska/northern Canada, ambient noise at these periods arrives mainly from the south, presumably along the Pacific coast of Canada and Alaska. In the eastern

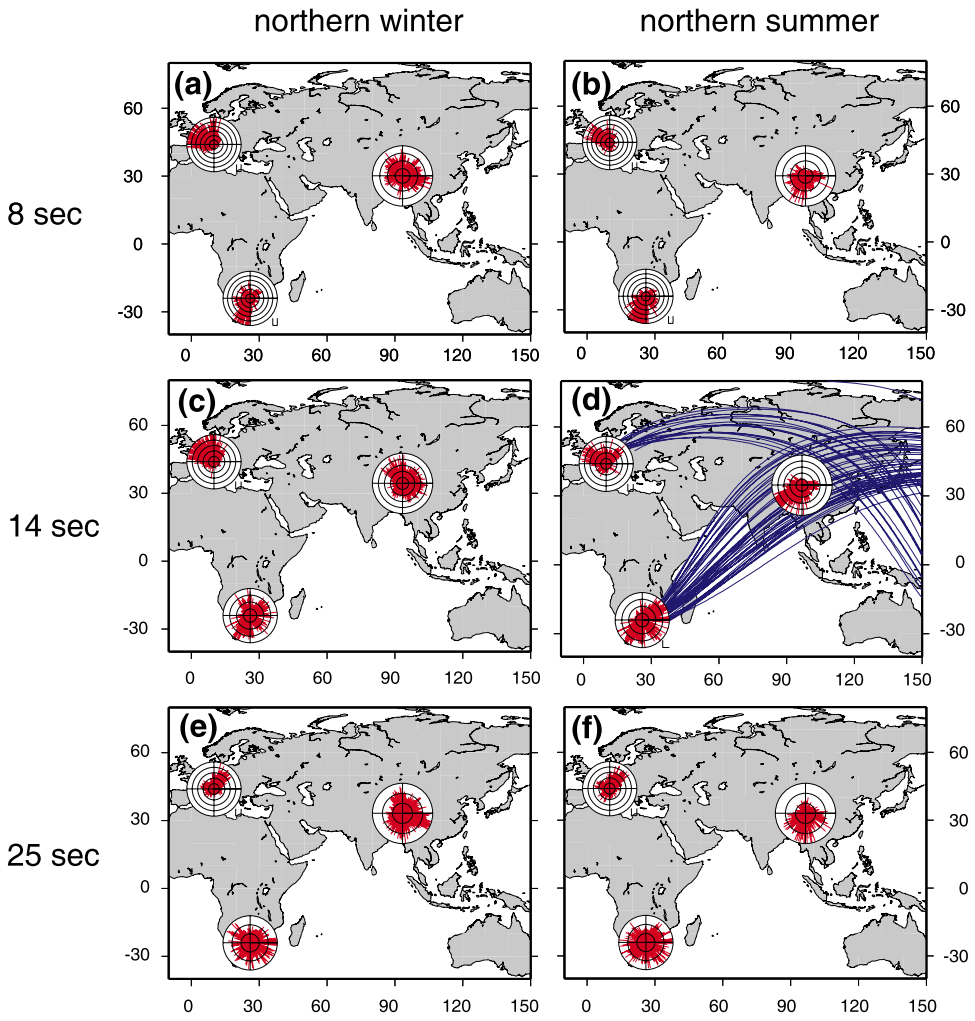

Figure 9. Similar to Figure 6 but here the azimuthal distribution of SNR of 5-month stacks at periods (a and b) 8, (c and d) 14, and (e and f) 25 s in southern Africa and Tibet during the northern winter (Figures 9a, 9c, and 9e) and summer (Figures 9b, 9d, and 9f) are compared with results from Europe. SNR levels in each region are indicted by the concentric circles that are scaled in multiples of 20. Paths in Figure 9d are back-projected great circle curves with SNR > 60.

United States, in contrast, ambient noise arrives mainly from the northeast and west, i.e., either from the Canadian Atlantic coast or the Pacific coast of North America. Thus, at these locations there is no evidence of significant differences in the source locations at 8 and 14 s period.

[26] In the microseismic bands in California, the results are somewhat more complicated, however. At 8 s, there is weak seasonal variability with stronger waves arriving from the northwest in winter than in summer. At 14 s, the seasonal variation is strong and the 8 s and 14 s azimuthal patterns differ from one another. In the northern winter, the strongest signals arrive to California from the northwest and northeast at 14 s, presumably arriving from the northern Pacific and northern Atlantic coasts of North America. In the northern summer, however, the strongest arrivals are from the south and southwest, with the source locations probably being localized to the nearby coasts. These patterns are different from those at 8 s period, in which the dominant arrivals are in the southwest quadrant throughout the year, similar to the azimuthal distribution at 14 s period during the northern summer. *Stehly et al.* [2006] argue from a similar observation for the physical decoupling of the primary and secondary microseisms. Consistent with our observations in other regions, we believe the explanation is that these arrivals at 14 s period are coming from North American coastlines in the north Pacific and north Atlantic which are too far to be observed well at 8 s period.

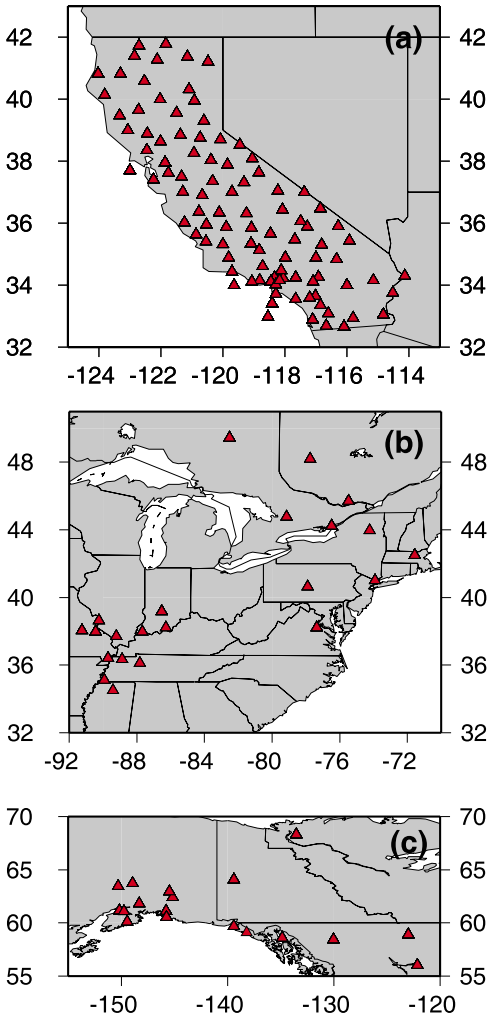

Figure 10. Stations used in North America.

[27] At 25 s period across North America, the azimuthal patterns are largely seasonally invariant with the most energetic waves apparently coming from the Pacific coast of the western United States.

[28] Thus, from microseismic band to longer-period ambient noise in North America, these results are consistent with near-coastal sources similar to our observations in the Eastern Hemisphere. The observed differences in directivity at 8, 14 and 25 s can be attributed to propagation and attenuation, rather than the location of generation.

6. Azimuthal Coverage and Recovery of Empirical Green's Functions

[29] In most theoretical treatments of ambient noise tomography and coda wave interferometry, the assumption of a perfectly homogeneous azimuthal distribution of noise sources is made [e.g., *Snieder*, 2004]. The observed distribution of ambient noise is far from homogeneous, however, with exceptionally strong signals sometimes emanating only from a narrow range of azimuths. Therefore questions have been raised [e.g., *Rhie and Romanowicz*, 2006] about the effect that this will have on the emergence of accurate empirical Green's functions from cross correlations of ambient noise and whether the observations can be used meaningfully to obtain dispersion measurements and perform tomography.

[30] This question has been addressed observationally in previous studies [e.g., *Shapiro et al.*, 2005; *Yang et al.*, 2007; *Lin et al.*, 2008; *Moschetti et al.*, 2007; *Bensen et al.*, 2007a, 2007b] using several lines of evidence. These studies showed that the observed interstation empirical Green's functions are similar to earthquake signals when earthquakes occur near to one of the stations, that dispersion curves are seasonally repeatable even though ambient noise characteristics may change substantially, and that the dispersion curves are consistent with one another even when azimuths are quite different. In addition, they showed that the resulting group and phase velocity maps reproduce geological structures faithfully. These and other reasons help to establish the veracity of ambient noise tomography. It should be borne in mind, however, that considerable efforts are exerted in processing ambient noise data to identify bad measurements (commonly more than half of all observations), some of which result from low signal levels or incomplete constructive/destruction interference in the generation of the observed Green's functions.

[31] The established veracity of ambient noise tomography appears, however, to be in conflict with the existence of relatively narrow azimuthal ranges with extraordinarily large amplitudes of ambient noise (e.g., Figures 12a–12c). Figures 12d–12f, which presents histograms of the number of 12-month European interstation cross correlations with SNR > 10 on either the positive or negative component, illustrates why this is not contradictory. The reason is that signals with SNR > 10 emerge from a wide range of azimuths. Only the very strongest signals are azimuthally limited. Thus, although there are preferred directions for ambient noise, predominantly at very short periods, significant ambient noise signals exist at a wide range of azimuths. The reason for this can be understood in terms of the interpretation that ambient

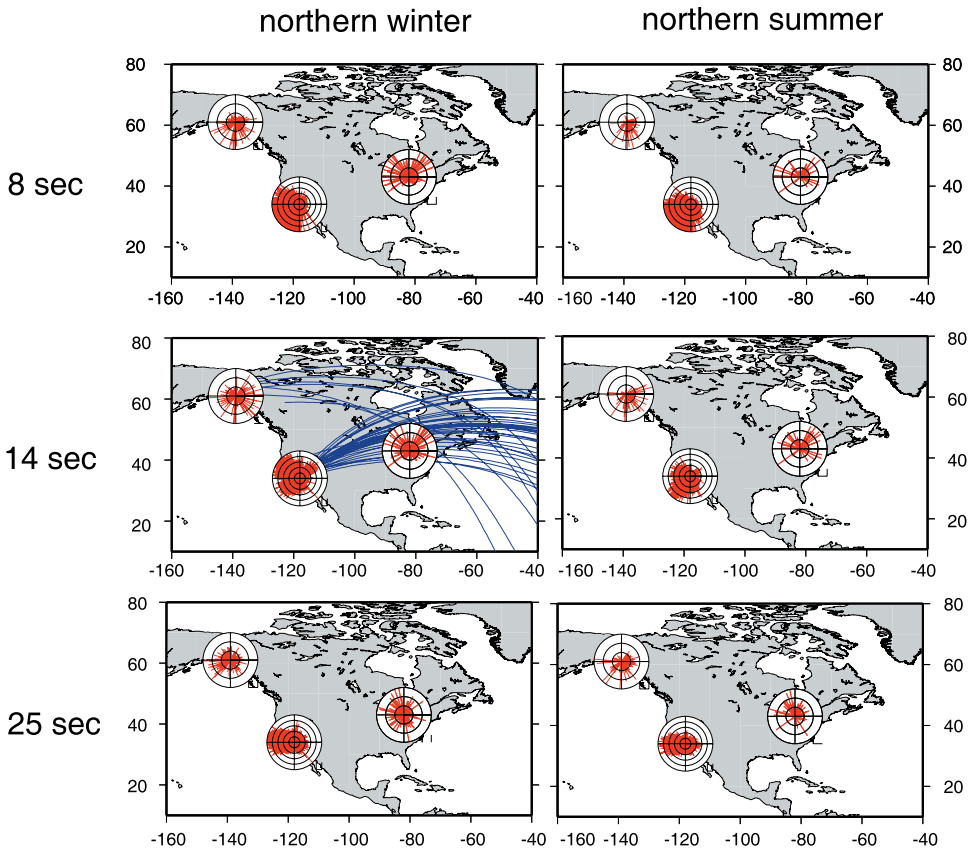

Figure 11. Same as Figure 6 but for stations in the North America: California, the eastern United States, and Alaska/Canada.

seismic noise is generated in shallow near coastal water.

[32] In order to demonstrate that accurate empirical Green's functions are obtained from long time noise series when ambient noise sources have an inhomogeneous azimuthal distribution with strong sources in some preferential directions, we present four synthetic experiments with different noise energy distributions. Synthetic sources are randomly distributed in a circular region with a diameter of 4000 km and a pair of stations are placed 450 km apart (Figure 13a). Each synthetic source emits a wavelet at a random initial time and at a random location with frequency content dominantly between about 15 and 25 s period. The waveform of the wavelet is the second derivative of a Gaussian function with a 20 s standard deviation. The wave velocity inside the circular region is 3 km/s everywhere. For each experiment, we run 30 simulations for each individual day totaling 30 d. For each day, 6000 sources are randomly distributed, but source energy has an azimuth-dependent distribution as shown in Figures 13b–13e. The resulting cross correlations are 30-d stacks. The empirical Green's functions, which are the negative time derivatives of the resulting cross correlations [*Snieder*, 2004], are plotted in Figure 14a with the theoretical Green's function plotted at the bottom as comparison. The resulting SNR for the simulations is similar to empirical Green's functions obtained for real data.

[33] In experiment I, the distribution of sources is azimuthally homogenous. Thus the cross correlation is nearly symmetric. In experiment II, there is stronger source energy coming from the right, which makes the cross correlations highly asymmetric with a much higher signal-noise-ratio on the positive component. In experiment III, stronger source energy comes from the northeast direction, similar to the incoming directions observed in Europe at 30 s period (Figure 12c) for stations oriented west-east. The resulting cross correlation is nearly symmetric because the strong sources from the northeast interfere with each other *destructively*. In experiment IV, stronger source energy comes from the forth quadrant, which

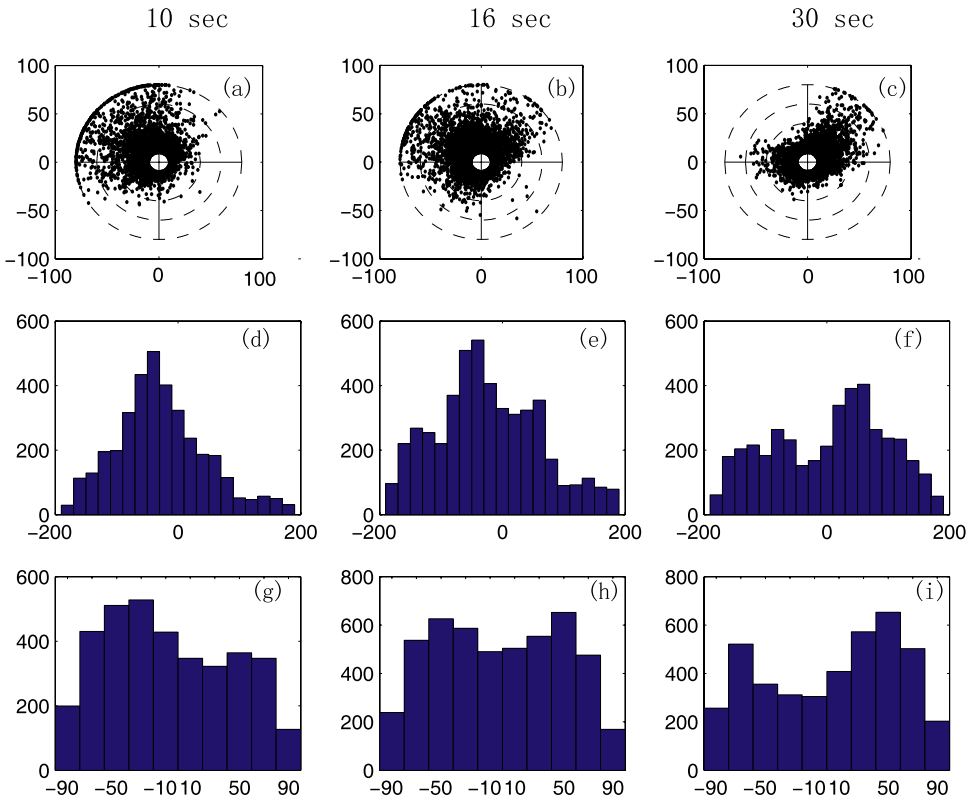

Figure 12. (top) Azimuthal distributions and (middle) histograms of the incoming directions of ambient noise. SNR levels are indicated by dashed concentrated circles with values denoted. (bottom) Histograms of bearing angles for cross correlations with SNR > 10 at 10, 16 and 30 s. Bearing angles are defined as the angle between the orientation of a path segment and the northern direction.

resembles the source distribution we observe at periods of 8 and 14 s in Europe (Figure 12a). The resulting cross correlation is asymmetric with a much higher signal-noise-ratio on the negative component. Arrival times of the peak energy at both positive and negative lags of the four cross correlations are about 150 s, which is the actual time for the wave to propagate between the two stations. We follow *Lin et al.* [2008] and obtain phase velocity measurements for the retrieved cross correlations by automatic frequency-time analysis (FTAN). The measured phase velocities and travel times are close to the input phase velocity (3 km/s) and travel time (150 s) with error less than about 0.5% at all periods (Figures 14b and 14c). The maximum travel time error (<2/3 s) is less than measurements errors with real data and considerably less than the RMS of data misfit in ambient noise phase velocity tomography [e.g., *Lin et al.*, 2008, Yang et al., submitted manuscript, 2007].

[34] These four synthetic experiments show that if ambient noise exists over a broad azimuthal range even at relatively low levels, accurate empirical Green's functions will emerge from long time series of the ambient noise even when the distribution is far from azimuthally homogenous. We have also conducted numerical experiments with random sources confined to an annulus with the radius of the inner circle equal to one fourth of the radius of the outer circle. The source azimuthal distributions for these experiments are the same as those shown in Figures 13b–13e. These experiments resemble the circumstances that the locations of ambient noise are distant relative to seismic stations. The results from these numerical experiments are almost identical, respectively, to those four cases shown in Figure 13. These numerical experiments imply that the resulting cross correlations of ambient noise are determined by the relative azimuthal distributions rather than detailed lateral distributions of sources.

[35] With the results from the synthetic experiments in mind, Figures 12g–12i provide additional insight into why ambient noise tomography works so well. It presents bearing angles of path segments for the selected cross correlations at periods of 10, 16 and 30 s. Bearing angles are defined as the angle between the orientation of a path segment

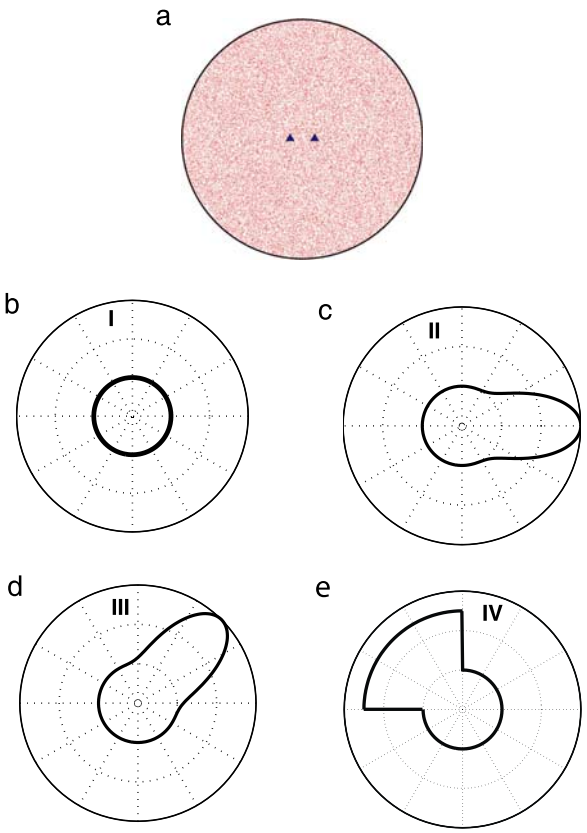

Figure 13. (a) Circular region with a diameter of 4000 km for the noise simulation. Each red dot represents a randomly distributed source. The two blue triangles are the two receiver stations placed 450 km apart. (b–e) Azimuthal distributions of the strength of source energy delineated by the bold lines for experiments I, II, III, and IV, respectively.

and the northern direction with a range between −90° and 90° because, for any cross correlation, positive and negative components with noise coming from two opposite directions have the same orientation. Although there is a slight preponderance of paths striking northwest-southeast across Europe, particularly at short periods, the distribution is strikingly homogeneous, which is good for the emergence of accurate empirical Green's functions and for resolution in surface wave tomography, particularly for extracting information about azimuthal anisotropy. These observations provide another line of evidence that highlights the advantage of ambient noise in providing homogenous ray coverage in surface wave tomography.

7. Conclusions

[36] Three principal questions have motivated this study. (1) Does the directivity of ambient noise provide evidence that the primary and secondary microseisms are physically decoupled? (2) Is ocean-produced ambient seismic noise generated in relatively shallow near-coastal waters or in deep water at longer periods? (3) Is the azimuthal distribution of ambient noise sufficiently homogeneous to allow for the retrieval of largely unbiased empirical Green's functions? We addressed each of these questions by investigating the strength and azimuthal distribution of ambient noise between 8 and 50 s period in Europe, southern Africa, Tibet, and three regions in North America (California, Alaska/northern Canada, eastern United States). Because the methods we use recover information only about the direction to strong ambient noise sources and not their absolute locations, the results are not entirely unambiguous. The inferences that we draw, therefore, are based also on appealing to the principle of simplicity.

[37] First, we find no compelling evidence for difference in source locations of the primary and secondary microseisms. The seasonal variation of the two microseisms is similar in all regions that we studied. Although the azimuthal distributions of the two microseisms do vary in some places, this difference is most simply attributable to the fact that the primary microseismic wave can propagate coherently over much longer distances than the secondary microseismic wave. It is possible and probably likely, however, that the relative amplitude of the primary and secondary microseisms upon generation of these waves is globally variable. However, characterizing the regional variation of this ratio is beyond the scope of this paper.

[38] Second, in all studied regions and at all periods studied here (8–50 s) the most simple location for the source of ambient noise lies in near-coastal waters. Deep water sources cannot be formally ruled out by the methods we apply here. We show, however, that deep water source regions would have to cover much of the ocean basins, which we argue is unlikely. In addition, source directivity at long periods on different continents differs, and, therefore, there is no evidence for common source locations in deep water.

[39] Third, and perhaps surprisingly, ambient noise emerges in each of the studied regions at a broad range of azimuths. If this does appear surprising it is probably because studies of ambient noise typically have focused on characterizing the strongest ambient noise directions, which are limited in azimuth. Even though the strongest noise emerges only from a few directions in most places, strong

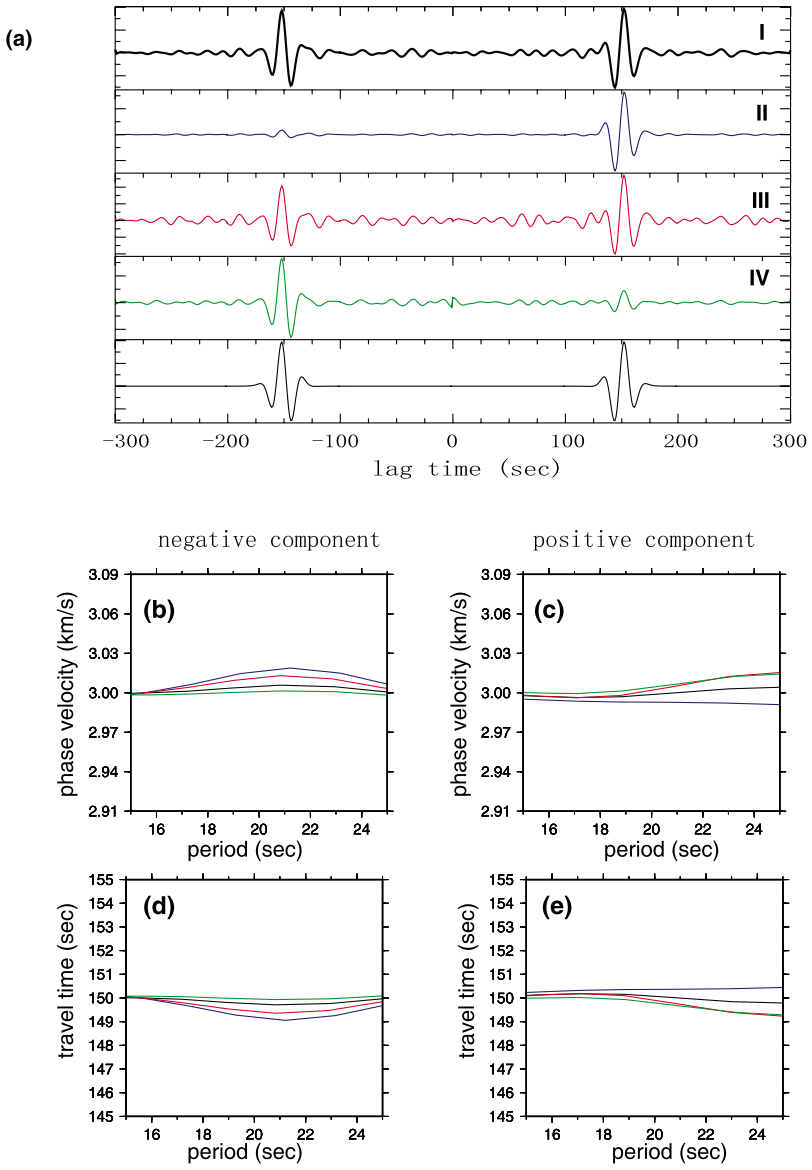

Figure 14. (a) Normalized empirical Green's functions (EGFs) from synthetic cross correlations for experiments I, II, III, and IV. At bottom is the theoretical Green's function. (b and c) Phase velocity measurements obtained on the normalized EGFs for negative and positive components, respectively. (d and e) Travel times at various periods for EGFs. The black line is for experiment I, the blue line is for experiment II, the red line is for experiment III and the green line is for experiment IV. Input phase velocity is 3 km/s, and travel time is 150 s.

ambient noise emerges from many directions. Thus, for the orientation of most station pairs, sufficiently strong ambient noise is present to be the basis for the retrieval of reliable empirical Green's functions. Nevertheless, there are some azimuths in most regions where ambient noise is so weak that interstation cross correlations will not provide a good empirical Green's function. From a practical perspective, therefore, these cross correlations have to be identified and removed as candidate empirical Green's functions. Typically, these cross correlations have a low signal-to-noise ratio, and SNR is useful in the data processing part of ambient noise tomography to identify the acceptable empirical Green's functions [e.g., *Bensen et al.*, 2007a]. The principal caveat is that there are some exceptionally strong spurious signals, such as the persistent 26 s resonance in the Gulf of Guinea [*Shapiro et al.*, 2006], that require dedicated data processing to remove [*Bensen et al.*, 2007a].

[40] In closing, the ways in which the strength and distribution of ambient noise vary in both azimuth

and region appear to be consistent generally with the hypothesized generation of ambient noise advocated by *Rhie and Romanowicz* [2006]. In this scenario, wind energy is converted to ocean wave energy in the deep oceans. Ocean wave energy is then transported to the fringes of continents as ocean gravity waves (or so-called infragravity waves at longer periods). Near coastlines, ocean gravity waves convert to solid earth propagating seismic waves when water is shallow enough to allow their direct interaction with the seafloor. The primary and secondary microseisms are physically coupled through a nonlinear, frequency-doubling process resulting from wave-wave interactions between the direct and coastally reflected waves.

[41] It may not be generally appreciated that this mechanism would predict that ambient noise is well distributed in azimuth. Ocean gravity waves generated in deep water will propagate to coastlines broadly across the ocean basin where seismic waves will be generated over a large area in relatively shallow water. This mechanism also would predict that the strongest seismic waves would be generated when and where the storm intersects the coastline. Both of these predictions, the broad area of generation of ambient noise along coastlines and the strongest waves emanating from only a few azimuths, are consistent with our observations. Given the ambiguities inherent in the methods applied herein, however, we view these results as relatively weak confirmation of the hypothesized mechanism of Rhie and Romanowicz. More direct observations are needed to test this hypothesis further.

Acknowledgments

[42] The data used in this research were downloaded from the continuous ftp database of the Orfeus (Observatories and Research Facilities for European Seismology) Data Center and from the IRIS Data Management Center. The authors are deeply grateful to the networks that contribute data to the Virtual European Broadband Seismic Network (VEBSN), a partnership of more than 30 local, regional and global arrays and networks. In addition, the authors would like to acknowledge two PASSCAL experiments that provided data for this research: the Southern Africa Seismic Experiment and the Eastern Syntaxis Tibet Experiment. The authors gratefully acknowledge Barbara Romanowicz, another anonymous reviewer and Editor John Tarduno for comments that improved the manuscript. This research was supported by U.S. National Science Foundation grant EAR0711526 and U.S. Department of Energy contract DE-FC52-2005NA26607.

References

Aki, K., and B. Chouet (1975), Origin of coda waves: Source, attenuation, and scattering effects, *J. Geophys. Res.*, *80*, 3322–3342.

Bensen, G. D., M. H. Ritzwoller, M. P. Barmin, A. L. Levshin, F. Lin, M. P. Moschetti, N. M. Shapiro, and Y. Yang (2007a), Processing seismic ambient noise data to obtain reliable broad-band surface wave dispersion measurements, *Geophys. J. Int.*, *169*, 1239–1260, doi:10.1111/j.1365-246X.2007.03374.x.

Bensen, G. D., M. H. Ritzwoller, and N. M. Shapiro (2007b), Broad-band ambient noise surface wave tomography across the United States, *J. Geophys. Res.*, doi:10.1029/2007JB005248, in press.

Cho, K. H., R. B. Herrmann, C. J. Ammon, and K. Lee (2007), Imaging the upper crust of the Korean Peninsula by surface-wave tomography, *Bull. Seismol. Soc. Am.*, *97*, 198–207.

Derode, A., E. Larose, M. Campillo, and M. Fink (2003a), How to estimate the Green's function of a heterogeneous medium between two passive sensors? Application to acoustic waves, *Appl. Phys. Lett.*, *83*, 3054–3056.

Derode, A., E. Larose, M. Tanter, J. de Rosny, A. Tourim, M. Campillo, and M. Fink (2003b), Recovering the Green's function from field-field correlations in an open scattering medium, *J. Acoust. Soc. Am.*, *113*, 2973–2976.

Ekstrom, G. (2001), Time domain analysis of Earth's longperiod background seismic radiation, *J. Geophys. Res.*, *106*, 26,483–26,493.

Gudmundsson, O., A. Khan, and P. Voss (2007), Rayleigh-wave group-velocity of the Icelandic crust from correlation of ambient seismic noise, *Geophys. Res. Lett.*, *34*, L14314, doi:10.1029/2007GL030215.

Hasselmann, K. (1963), A statistical analysis of the generation of microseisms, *Rev. Geophys.*, *1*, 177–210.

Larose, E., A. Derode, D. Corennec, L. Margerin, and M. Campillo (2005), Passive retrieval of Rayleigh waves in disordered elastic media, *Phys. Rev. E*, *72*, 046607, doi:10.113/PhysRevE.72.046607.

Lin, F., M. H. Ritzwoller, J. Townend, M. Savage, and S. Bannister (2007), Ambient noise Rayleigh wave tomography of New Zealand, *Geophys. J. Int.*, *170*, 649–666, doi:10.1111/j.1365-246X.2007.03414.x.

Lin, F., M. P. Moschetti, and M. H. Ritzwoller (2008), Surface wave tomography of the western United States from ambient seismic noise: Rayleigh and Love wave phase velocity maps, *Geophys. J. Int.*, in press.

Longuet-Higgins, M. S. (1950), A theory on the origin of microseisms, *Philos. Trans. R. Soc. London*, *243*, 1–35.

Moschetti, M. P., M. H. Ritzwoller, and N. M. Shapiro (2007), Surface wave tomography of the western United States from ambient seismic noise: Rayleigh wave group velocity maps, *Geochem. Geophys. Geosyst.*, *8*, Q08010, doi:10.1029/2007GC001655.

Nawa, K., N. Suda, Y. Fukao, T. Sato, Y. Aoyama, and K. Shibuya (1998), Incessant excitation of the Earth's free oscillations, *Earth Planets Space*, *50*, 3–8.

Paul, A., M. Campillo, L. Margerin, E. Larose, and A. Derode (2005), Empirical synthesis of time-asymmetrical Green functions from the correlation of coda waves, *J. Geophys. Res.*, *110*, B08302, doi:10.1029/2004JB003521.

Rhie, J., and B. Romanowicz (2004), Excitation of Earth's continuous free oscillations by atmosphere-ocean-seafloor, *Nature*, *431*, 552–556.

Rhie, J., and B. Romanowicz (2006), A study of the relation between ocean storms and the Earth's hum, *Geochem. Geophys. Geosyst.*, *7*, Q10004, doi:10.1029/2006GC001274.

Sabra, K. G., P. Gerstoft, P. Roux, W. A. Kuperman, and M. C. Fehler (2005), Surface wave tomography from microseism in southern California, *Geophys. Res. Lett.*, *32*, L14311, doi:10.1029/2005GL023155.

Shapiro, N. M., and M. H. Ritzwoller (2002), Monte-Carlo inversion for a global shear velocity model of the crust and upper mantle, *Geophys. J. Int.*, *151*, 88–105.

Shapiro, N. M., M. Campillo, L. Stehly, and M. H. Ritzwoller (2005), High resolution surface wave tomography from ambient seismic noise, *Science*, *307*, 1615–1618.

Shapiro, N. M., M. H. Ritzwoller, and G. D. Bensen (2006), Source location of the 26 sec microseism from cross correlations of ambient seismic noise, *Geophys. Res. Lett.*, *33*, L18310, doi:10.1029/2006GL027010.

Snieder, R. (2004), Extracting the Green's function from the correlation of coda waves: A derivation based on stationary phase, *Phys. Rev. E*, *69*, 046610.

Stehly, L., M. Campillo, and N. M. Shapiro (2006), A study of the seismic noise from its long range correlation properties, *J. Geophys. Res.*, *111*, B10306, doi:10.1029/2005JB004237.

Tanimoto, T. (2005), The oceanic excitation hypothesis for the continuous oscillations of the Earth, *Geophys. J. Int.*, *160*, 276–288.

Tanimoto, T., and J. Um (1999), Cause of continuous oscillations of the Earth, *J. Geophys. Res.*, *104*, 28,723–28,739.

Weaver, R. L., and O. I. Lobkis (2001), On the emergence of the Green's function in the correlations of a diffuse field, *J. Acoust. Soc. Am.*, *110*, 3011–3017.

Weaver, R. L., and O. I. Lobkis (2004), Diffuse fields in open systems and the emergence of the Green's function, *J. Acoust. Soc. Am.*, *116*, 2731–2734.

Webb, S. C. (1998), Broadband seismology and noise under the ocean, *Rev. Geophys.*, *36*, 105–142.

Yang, Y., M. H. Ritzwoller, A. L. Levshin, and N. M. Shapiro (2007), Ambient noise Rayleigh wave tomography across Europe, *Geophys. J. Int.*, *168*, 259–274.

Yao, H., R. D. van der Hilst, and M. V. De Hoop (2006), Surface-wave array tomography in SE Tibet from ambient seismic noise and two-station analysis: I—Phase velocity maps, *Geophys. J. Int.*, *166*, 732–744.